Using Random Forests to Compare the Sensitivity of Observed Particulate Inorganic and Particulate Organic Carbon to Environmental Conditions

Rui Jin[1], Anand Gnanadesikan[1], and Christopher Holder[1]

[1] Department of Earth and Planetary Sciences, Johns Hopkins University, Baltimore, Maryland, USA

Corresponding author: Rui Jin (ruijin@jhu.edu)

Key Points:

- Particulate inorganic and organic carbon (PIC and POC) estimated from satellites can be predicted using environmental conditions.
- Random forests produce similar nonlinear relationships between some environmental factors (i.e. ammonium) and PIC and POC.
- PIC is less sensitive to iron and more sensitive to light and mixed layer depth than POC.

Abstract

The balance between particulate inorganic carbon (PIC) and particulate organic carbon (POC) holds significant importance in carbon storage within the ocean. A recent investigation delved into the spatial distribution of phytoplankton and the physiological mechanisms governing their growth. Employing random forests, a machine learning technique, this study unveiled apparent relationships between POC and 10 environmental fields. In this work, we extend the use of random forests to compare how observed PIC and POC respond to environmental conditions. Our findings indicate that while both exhibit similar responses to certain environmental drivers, PIC is less sensitive to iron and more sensitive to light. Intriguingly, both PIC and POC display reduced sensitivity to CO_2, contrary to previous studies, possibly due to the elevated pCO_2 in our dataset. This research sheds light on the underlying processes influencing carbon sequestration and ocean productivity.

Plain Language Summary

This study looks at how different types of carbon, specifically tiny particles of chalk (particulate inorganic carbon, PIC) and organic carbon from microscopic marine plants (particulate organic carbon, POC), are distributed in the ocean and how they respond to environmental conditions. The ratio between PIC and POC has a big impact on how carbon is stored in the ocean. We used a machine learning technique to analyze how patterns in these fields estimated from satellite were related to drivers such as light and nutrients. We found that PIC and POC react similarly to some environmental factors (such as ammonium) but differently to others (such as iron and light). Surprisingly, both types of carbon showed less sensitivity to CO_2 than expected from previous work, possibly because of high CO_2 levels in the dataset.

1 Introduction

Because different phytoplankton functional types (PFTs) are associated with different elemental cycles there is thus a need to understand how PFTs respond to different environmental drivers. In particular, the ratio of particulate inorganic carbon (PIC) to particulate organic carbon (POC) can play a pivotal role in the oceanic storage of carbon. POC primarily originates from phytoplankton photosynthesis, resulting in the conversion of CO_2 into organic compounds and consequent sequestration of CO_2 from the marine environment. Each year, nearly 10 gigatons of carbon are exported from the ocean surface while around 2000 gigatons of carbon are stored in the deep ocean through the biological pump (Boyd et al., 2019). However, the production of PIC by calcifying planktonic organisms (e.g., coccolithophores) results in an opposing effect on surface water pCO_2 as the accompanying reduction in seawater alkalinity leads to the release of CO_2 (Liang et al., 2023; Kwon et al., 2009).

Extensive investigations have focused on deciphering the attributes of the PIC:POC ratio to unravel the ramifications of global climate change on the dynamics of the oceanic carbon cycle (Sarmiento et al., 2002; Rivero-Calle et al., 2015; Krumhardt et al., 2017). Archer et al. (2000) argue that a decline in the PIC:POC export ratio may have contributed to the reduction in atmospheric CO_2 that occurred during the last ice age. Brovkin et al. (2019) suggest that the increase in atmospheric CO_2 during the Holocene was associated with changes in the rain ratio and carbonate burial. Because of this, gaining a comprehensive understanding of the distributional characteristics and sensitivities of PIC in comparison to POC is essential for improved modeling of marine ecosystems and their responses to environmental changes.

In a recent investigation, Holder and Gnanadesikan (2021) utilized machine learning techniques to reveal apparent relationships between the spatial distribution of phytoplankton and the physiological mechanisms controlling their growth. These apparent relationships (those found in the environment where many environmental drivers co-vary and where many species are present) are different from intrinsic relationships found in laboratory settings where one variable at a time is considered, usually for one species. Holder and Gnanadesikan (2023, henceforth HG23) found that a large fraction of variability in observations can be linked to large-scale environmental variables via these apparent relationships. The dominant predictors in the observational data sets of POC were shortwave radiation and dissolved iron, with temperature and ammonium also relatively important. However, they did not consider the impact of different physiological mechanisms on different types of phytoplankton.

The present study juxtaposes the apparent relationships between environmental drivers of global PIC and POC, allowing an assessment of how the spatiotemporal distributions of POC and PIC are controlled differently. Our findings demonstrate PIC and POC exhibit distinct sensitivities to variations in light, iron, and mixed layer depth.

2 Methods

2.1 Observations

A large portion of the observational data used in our analysis was compiled as part of the HG23 manuscript. For clarity and to minimize the requirements of the reader to seek out additional scientific papers, we provide a brief overview of how the observations were compiled in HG23 below. For additional information on the dataset construction, please see HG23.

We employed observational datasets based on remote sensing as target datasets. Using remotely sensed data does introduce potential sources of error into our analytical framework, as the algorithms used to generate these products may be biased. However, using satellite-based measurements is integral to our research objectives. First, this enables the sampling of a wide range of environmental conditions while maintaining measurement consistency, thereby optimizing the identification of variables that explain a substantial proportion of variance. Second it facilitates the generation of datasets that are large enough for applying tree-based analytical methods designed to uncover nonlinear relationships.

The first of these datasets was the MODIS-Aqua POC product (Stramski, et al. 2008). This particular dataset predicts POC concentrations from the remote sensing reflectances Rrs measured at wavelengths of 443 and 555 nm using the equation:

$$POC = A_1[R_{rs}(443)/R_{rs}(555)]^{B_1}$$

Where A_1 and B_1 are regression coefficients.

The second target dataset utilized in our study was PIC product from Balch et al. (2005) and Gordon et al. (2001). The PIC algorithm is a hybrid of two independent approaches, defined as the 2-band approach and the 3-band approach. The 2-band approach uses normalized water-leaving radiances in two bands near 443 and 555 nm. The 3-band approach uses spectral top-of-atmosphere reflectances at three wavelengths near 670, 750, and 870 nm.

We accessed both PIC and POC products with a spatial resolution of 9 km and a monthly climatology spanning from July 2002 to December 2022 from the NASA Ocean Color website. To enhance data quality and spatial coverage, we regridded both datasets to a spatial resolution of 1°.

2.2 Environmental drivers

HG23 sourced 1° monthly averaged, objectively analyzed, temperature, salinity, mixed layer depth, silicate, phosphate, and nitrate from the World Ocean Atlas (WOA) 2018 dataset (Garcia et al., 2019; Locarnini et al., 2019; Zweng et al., 2019). Monthly vertical velocity data at a depth of 55 meters were acquired from the Estimating the Circulation and Climate of the Ocean (ECCO) reanalysis dataset, version 4 release 4 (ECCO Consortium et al., 2021a, 2021b; Forget et al., 2015). Net shortwave radiation (QSW) at the ocean surface from the International Satellite Cloud Climatology Project (ISCCP) provided by the Objectively Analyzed Air-Sea Fluxes (OAFlux) Project (Yu et al., 2006),was used as a proxy for light supply as in accordance with the rationale outlined in HG23. We also use the globally interpolated MPI-ULB-SOMFFN climatological pCO_2 product (Landschützer et al. 2020b) as an additional environmental driver. No globally interpolated observational datasets are available for dissolved iron and ammonium, both sparsely sampled variables. To address this, HG23 generated synthetic "observational" datasets by utilizing the ensemble average of CMIP6 Earth System Models (ESMs). Both of these synthetic predictors ended up being important predictors of observed POC in HG23.

Phytoplankton can persist under low light levels, including high-latitude areas during winter, where they often enter a dormant state. Models are capable of sustaining low levels of biomass in such conditions. However, the observational datasets derived from passive satellite products lack information in these specific regions, resulting in an analytical gap. To address this limitation, we incorporated the low-light regions into our analysis by replacing missing months at points which had some measurements in the POC and PIC datasets with the 1st percentile value within the corresponding global dataset (while HG23 used the 5th percentile, this difference does not significantly impact the results).

2.3 Random Forest

Random Forest (RF) is a powerful ensemble learning technique widely employed in the field of machine learning (Breiman, 2001). It operates by constructing a multitude of decision trees during the training phase and outputs predictions based on the aggregate result of these individual trees. Each tree is built on a different subset of the dataset, using a subset of predictors. This contributes to its resilience against overfitting and enhances predictive accuracy. Renowned for its robustness and ability to handle diverse data types, RF has become a favored tool in predictive modeling, classification, and regression tasks across various domains.

To mitigate the risk of overfitting, we employed a random data splitting approach for both the PIC and POC datasets. The dataset was split into distinct training and testing subsets with 80%

of the values from each dataset allocated to the training subsets and the remaining 20% forming the testing subsets. This ensured that the testing subsets contained data unfamiliar to the RF models during their training phase. In accordance with arguments made in HG23, decision trees were constructed without sample replacement. The assessment of each RF model's performance was carried out using the testing data, which were presented as input to the trained models.

RF models were formulated for each of the satellite-based observational estimates. The target data consisted of logarithmically transformed POC or PIC variables. This transformation was employed to reduce the undue influence of exceptionally large values, given the highly skewed nature of both target variables. The predictor dataset, identified as "observational" for the RF models, comprised observed values for sea surface temperature (SST), sea surface salinity (SSS), shortwave radiation, nitrate, phosphate, silicate, pCO_2, reanalyzed values of upwelling velocity, and model-ensemble estimates for iron and ammonium. These datasets were standardized to a uniform 1° grid.

Since RFs employ a subset of variables for constructing each tree (in our case, 4 out of 11 predictors), it is imperative to ensure an adequate number of trees to capture the essential nonlinear interactions required to model the target variable effectively. A total of 50 decision trees were constructed for each RF, following the methods of HG23 who performed a metanalysis to identify the optimal settings. The increase in the relative error when comparing testing data and RF generated predicting data is relatively small (Table S1), suggesting the RFs perform relatively well, capturing 88.7% and 83.9% of the variance in the total POC and PIC datasets, respectively.

The assessment of variable importance within a dataset can be approached through various methodologies. One of these is referred to as the permutation method. The permutation method is a robust technique employed in statistical analysis and machine learning to assess the importance of predictor variables in a model. In this method, a baseline is initially established by calculating the model error using a trained algorithm, such as a RF. Subsequently, each predictor variable's influence is evaluated by introducing randomness – the variable values are shuffled, creating a modified dataset. This modified dataset is then presented to the trained model for predictions, and the disparity between the error of these new predictions and the original error is computed for each predictor variable. A substantial increase in the root mean squared error (RMSE) signals that a particular variable holds greater importance, highlighting its significance in the predictive process. Conversely, variables associated with marginal increments in error are considered less influential. The permutation method thus provides valuable insights into the relative importance of predictors.

Additionally, we conducted analyses involving the substitution of one predictor's value with its observed median, while keeping the other predictor values in accordance with their observed variations. This modified dataset was then presented to the RF model for analysis. A low prediction in regions where the predictor variable is below the median value implies the potential for this variable to suppress phytoplankton biomass.

Finally, in order to gain insights into the inherent relationships within each RF we conducted sensitivity analyses. These analyses involved an exploration of the influence of individual predictor variables. For example, when analyzing the sensitivity of iron, we adjusted its values to span the minimum and maximum range observed in the observational dataset. At the same time the other predictor variables were set to their median values (i.e. SW radiation was set to 176 W/m^2). This artificially constructed dataset was then supplied to the RF model to generate a “median sensitivity”.

3. Results and discussion

The distribution patterns of PIC and POC exhibit substantial disparities, both temporally and spatially, as evident in Figure 1. In Northern Hemisphere winter, PIC concentrations (Fig. 1a) demonstrate elevated levels in high-latitude regions of the Southern Hemisphere, gradually diminishing as one approaches approximately 30°S latitude. Subsequently, there is an increase in PIC concentrations near the equator, followed by a decline in values as latitudes increase in the Northern Hemisphere. In contrast, POC concentrations (Fig 1d) exhibit their lowest values in subtropical regions of both the Northern and Southern Hemispheres, with an augmentation observed around the equator and in latitudes exceeding 30°.

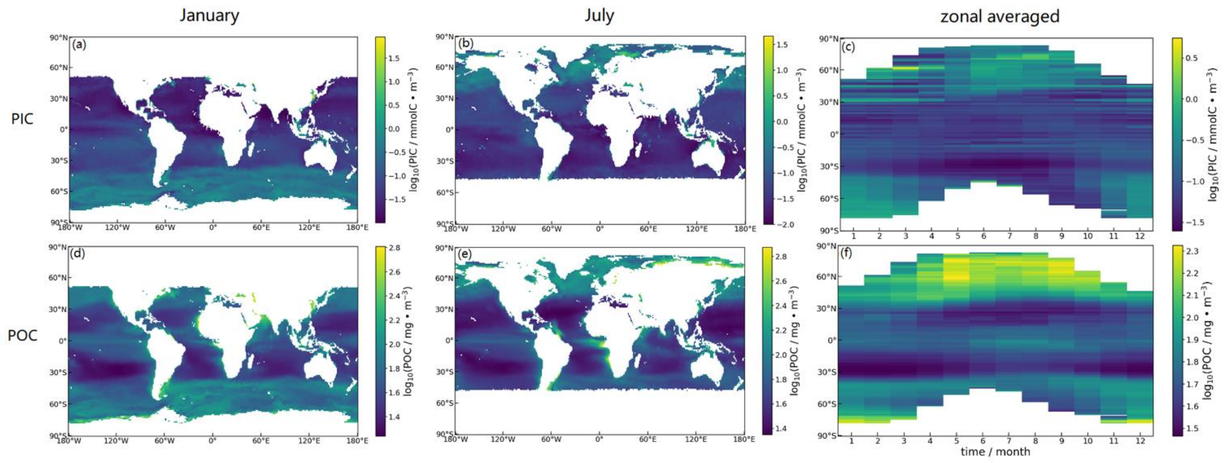

Figure 1. Global distribution of PIC and POC in January (1a and 1d) and July (1b and 1e) from the Moderate Resolution Imaging Spectroradiometer (MODIS) averaged over all days during the entire measuring period (2002-2022). The third column shows the zonal averaged PIC (1c) and POC (1f). Concentrations are in log scale for better contrast.

Figure 1e illustrates that POC distribution in July follows a similar zonal transition pattern as observed in January, albeit with different absolute values. Generally, POC concentrations in high-latitude areas of the Southern Hemisphere during July are lower compared to those in January, while concentrations in the Northern Hemisphere are higher. In contrast, the PIC concentration in July (Fig. 1b) displays a reverse pattern when contrasted with its distribution in January. During July, PIC concentrations are elevated in high-latitude regions of the Northern Hemisphere, gradually declining as latitudes approach 30°S, with a minor increase near the equator and reaching their lowest values in the Southern Hemisphere. Upon closer examination of these distribution patterns, it becomes apparent that POC concentrations tend to align more closely with the annual-mean wind stress curl field, whereas PIC concentrations are more tightly coupled to seasonal changes.

To gain deeper insights into the contrasting distribution patterns of PIC and POC, we present zonally-averaged concentrations (Fig. 1c, f). The distribution of POC concentration is characterized by two distinct mid-latitude bands of reduced values, potentially attributed to subsurface downwelling instigated by wind stress. Additionally, our analysis reveals that between 15 and 30 degrees in both hemispheres, PIC is high during the summer and low during the winter so that the peak of PIC concentration aligns with the solar zenith angle. This suggests potential correlations with light, temperature or the depth of the mixed layer. It is also notable that when we contrast POC and PIC in summer months for both hemispheres, a symmetry was observed in PIC around 30 degrees but was not seen for POC. Near-equatorial (15°S-15°N) regions show interesting differences. At 15°S, we can see a band of high values throughout the year. Additionally, we see a peak that moves northward during the spring, and southward during the fall, following the sun. POC shows a peak on the equator during Northern summer.

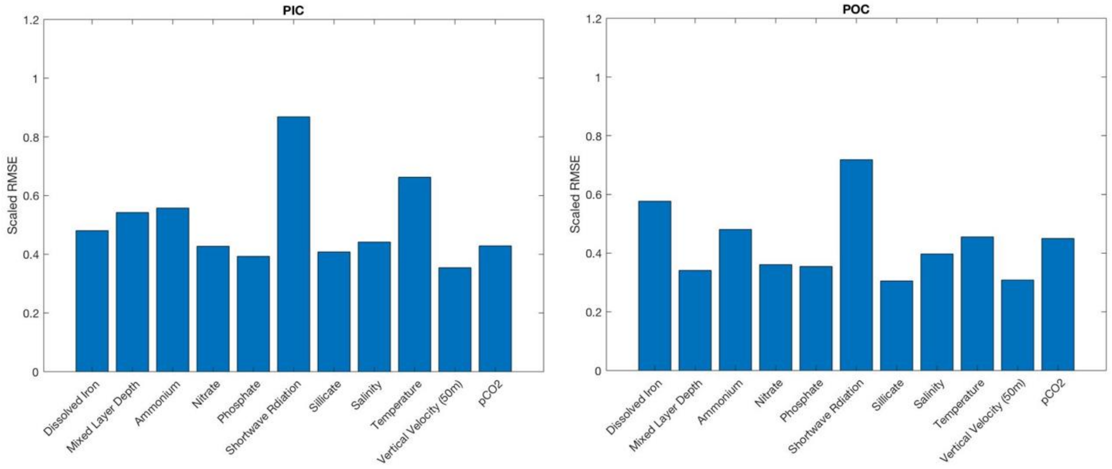

Figure 2. Variable importance plots for PIC (left) and POC (right) of the log10 transformed target datasets. The x-axis shows the variables that were used in each random forest (RF). The y-axis shows the relative importance of each variable computed by permuting each variable in the testing dataset with the others held at their observed values, computing the root mean squared error associated with the permuted inputs and normalizing this by the standard deviation of the target from each dataset.

To get a better sense of the underlying determinants of PIC and POC variability, the permutation importance (defined as the error when one variable is permuted for the testing data normalized by the standard deviation of target data) was computed for successive variables. Large error (RMSE) is indicative of predictors possessing greater importance, contributing significantly towards the predictions while small error means less importance. Plots are shown in Figure 2. Both datasets show that downward shortwave radiation is the most important variable. However, iron is the second-most important variable in the POC data set but is only the fifth most important in the PIC data set, ranking behind short wave radiation, temperature, mixed layer depth and ammonium. Mixed layer depth is more important for PIC than for POC. Salinity and vertical velocity are not very important in both datasets.

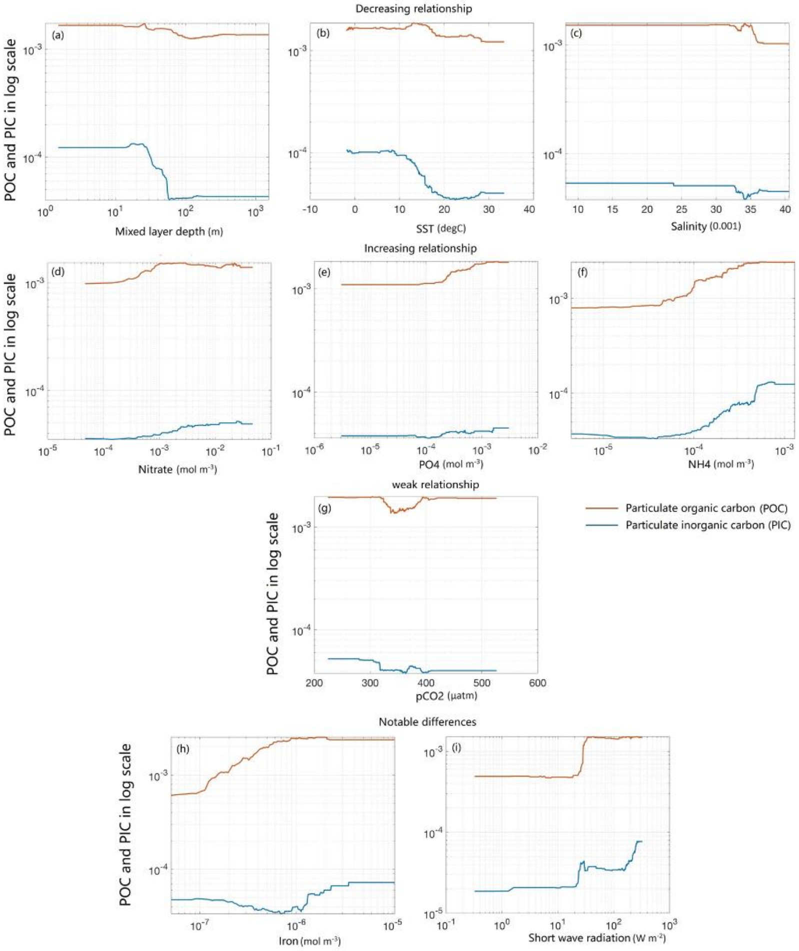

Figure 3. Sensitivity analyses on RFs trained on log10-transformed PIC (blue line) and POC (red line) target datasets. The minimum-maximum range for each variable was determined using values from the observational datasets and all other variables are set to their median value.

We then evaluate sensitivity of PIC versus POC to individual environmental parameters with all other variables fixed at their median. The first row shows that when increasing mixed layer depth, temperature and salinity (Fig. 3a, 3b and 3c), both PIC and POC remain relatively stable for some time then decrease at around the same concentration of the variable. For salinity, however, the drop in PIC reverses when salinity concentration increases to higher values. PIC is also more sensitive to changes in mixed layer depth than POC, consistent with the permutation importance in Fig. 2. Conversely, greater nitrate, phosphate and ammonium (Fig.3d, 3e and 3f) are associated with increases in both PIC and POC before plateauing at high values. Both PIC and POC are relatively insensitive to silicate and vertical velocity as shown in the supplement

(Fig. S1). Both POC and PIC show relatively weak, and inconsistent, responses to changes in pCO_2 (Fig. 3g).

Intriguingly, our investigation reveals distinct responses of PIC and POC to variations in iron and light consistent with Fig. 2. For dissolved iron (Fig. 3h), POC shows an increase with increasing iron before eventually plateauing while PIC shows a slight drop before returning to the previous values. As shown in Figure 3i, POC and PIC show similar patterns between values of 10 and 30 W/m^2, with a jump in each field observed as radiation increases. POC then reaches a plateau while PIC shows a second jump around 100 W/m^2 as shortwave radiation increases to higher values.

To elucidate the underlying mechanisms, we conducted a deeper examination of the spatial and temporal impacts of iron and light on PIC and POC. The influence of iron on the zonally averaged cycle of POC exhibits pronounced hemispheric asymmetry. In the Southern Hemisphere MODIS observations, low iron levels (Fig. 4a) suppress the summertime bloom, peaking in February at approximately 60°S with a 0.3 log unit reduction (roughly a factor of 2). Conversely, in the Northern Hemisphere MODIS observations, higher iron levels are associated with a stronger bloom, with peak enhancement occurring in May and June in subpolar latitudes, also roughly a factor of two. The zonally averaged cycle of PIC under the impact of iron displays different trends (Fig. 4b). Although reduced iron concentrations around the equator seem to suppress PIC consistently throughout the year (consistent with POC), the results show an opposite-sign sensitivity to iron compared to POC in other areas. In the Southern Hemisphere, spatiotemporal iron variability fosters a more robust PIC bloom, peaking around 60°S in February. In the Northern Hemisphere, higher iron levels suppress PIC around 50°S, particularly in March, while iron variability promotes a PIC bloom near the Arctic region.

The observed annual mean impact of iron (Fig. 4c) aligns with the zonally averaged cycle, revealing the most significant annual-mean biomass suppression (0.6 log units or a factor of 4) in the Southeast Pacific—a region known for low iron and biomass levels (Bonnet et al., 2008), as well as at the equator. Notably, higher iron emerges as a crucial factor in explaining elevated POC along the boundary of the subtropical/subpolar gyre in the North Pacific, North Atlantic, and the Arabian Sea. Conversely, the annual mean impact of iron on PIC has less of the ocean showing strong effects. More strikingly, the spatial pattern of PIC sensitivity to iron (Fig. 4d) is the opposite direction compared to POC in North Pacific, North Atlantic (particularly under the

Saharan dust plume) and Arabian Sea. Iron is associated with higher PIC levels in most parts of the Southern Ocean, as well as the South Pacific subtropical gyre.

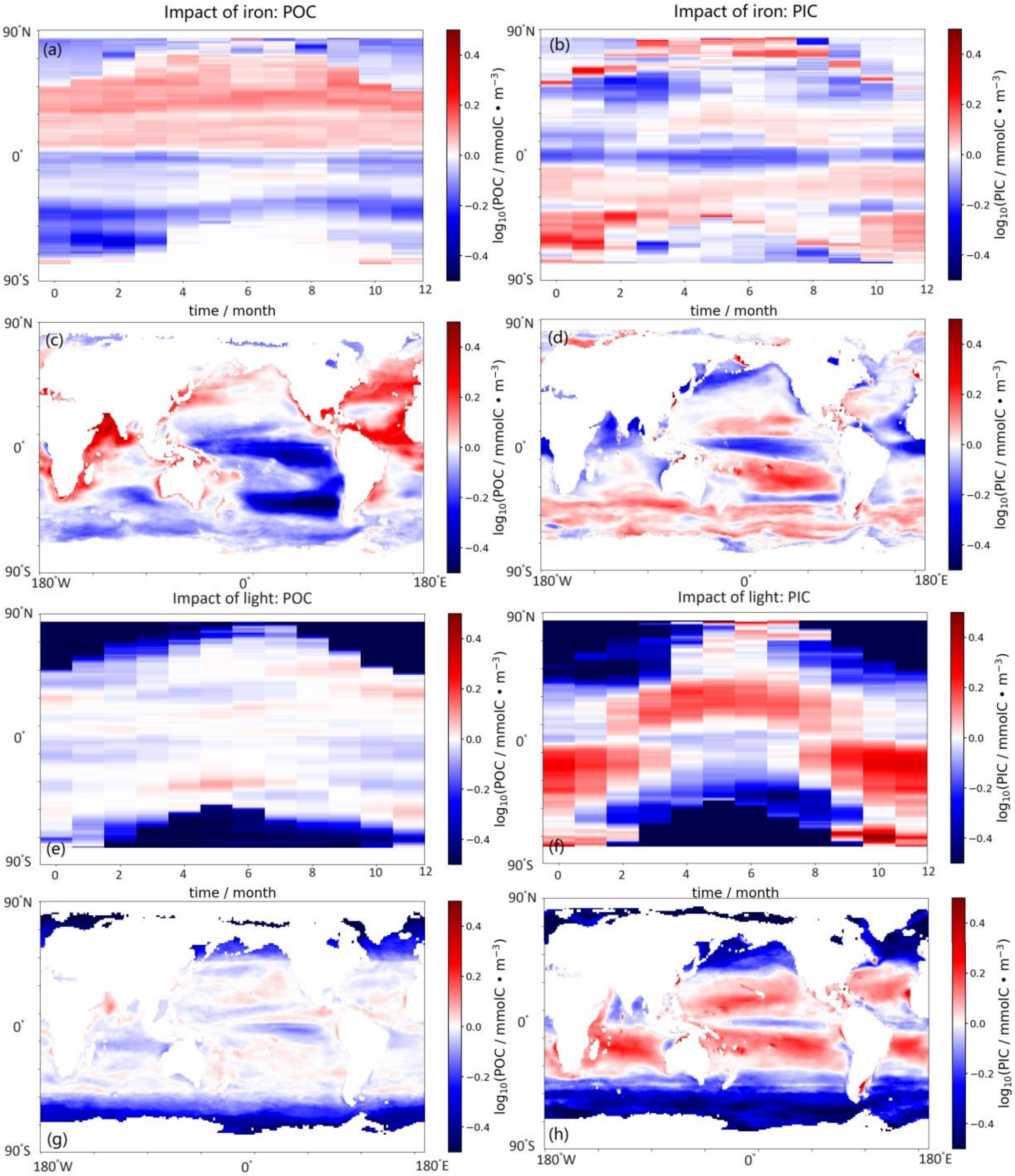

Figure 4. Impact of variability of iron or light on POC and PIC computed by replacing the observed/modeled value at each point in time and space by the median value from observations, running the RF for each dataset, and computing the difference between the RF using the observed/modeled value and that using the observed median. Scale is $\log_{10}$, so that a value of +0.1 means that the differences between the value of iron seen at that

latitude and longitude and the median value of iron increases biomass by $\log_{10}(0.1)$ or 26% when averaged across all months.

Compared to PIC, both the zonally averaged cycle and annual mean of POC exhibit weaker changes under the influence of light, with suppression observed at higher latitudes (Fig. 4e and f). This observation aligns with our findings in Figure 3. The zonally averaged cycle of PIC under the impact of light manifests clear hemispheric symmetry, with PIC blooms occurring in both hemispheres during summer.

4. Conclusions

In conclusion, our study highlights divergent sensitivities of PIC and POC to distinct drivers, with iron and light exhibiting particularly disparate impacts. Our findings align with the conclusions summarized by Krumhardt et al. (2017) that the sensitivity of POC and PIC to iron can be influenced by several factors, including temperature, CO_2 concentration, and the specific species of coccolithophore. This opposite-sign sensitivity suggests grazing dynamics might be different for PIC versus POC. In locations where sensitivity goes in the opposite direction, PIC-producers and non-PIC producers might have grazers in common, so that increases in the non PIC-producing phytoplankton would lead to more grazers and higher grazing pressure on the PIC-producing phytoplankton.

Our findings show evidence for different sensitivity to light and mixed layer depth. Specifically, as illustrated in Figure 3, PIC exhibits heightened sensitivity to light and mixed layer depth at higher ranges, surpassing the corresponding sensitivities of POC. Furthermore, our analysis, as depicted in Figure 4, demonstrates that the mean impact of light variability on PIC is notably more pronounced than that on POC. These findings align with Iglesias-Rodríguez et al. (2002)'s argument that a critical irradiance between 25 and 150 μmol quanta $m^{-2}\ s^{-1}$ selectively influences upper ocean large-scale coccolithophorid blooms.

Both the PIC and POC exhibit diminished sensitivity to CO_2 in contrast to observational syntheses made by Rivero-Calle et al. (2015) and Krumhardt et al. (2017). This divergence may be attributed to our examination of comparatively contemporary data characterized by elevated partial pressure of CO_2 (pCO_2) with concentrations from 325 to 407 ppmv representing the 5%-95% range in our dataset. In contrast, Rivero-Calle et al. (2015) only found growth rates falling when pCO_2 dropped below 300 ppmv, while Krumhardt et al. (2017) identified this decline at concentrations below 200 ppmv. Additionally, the disparity in findings may arise from the distinction in focus, with Krumhardt et al. (2017) concentrating on intrinsic relationships, whereas our investigation pertains to apparent relationships.

Future work should aim to deepen our understanding of the intricate interplay between iron, light and the dynamics of PIC and POC in marine ecosystems. Exploring the nuanced mechanisms governing the response of these carbon pools to varying environmental conditions will be crucial for refining predictive models and enhancing our ability to anticipate the repercussions of climate change on oceanic biogeochemistry. This supports the work of Krumhardt et al. (2017)

who pointed out a lack of conclusive physiological responses to irradiance changes and insufficient physiological data for major coccolithophore species.

Investigations into the specific physiological responses of key coccolithophore species to fluctuations in irradiance and iron availability could provide valuable insights into the underlying processes influencing carbon sequestration and ocean productivity. Long-term observational studies and the integration of advanced modeling techniques may further elucidate the complex relationships between environmental drivers and carbon cycling.

Acknowledgments: We thank Anastasia Romanou for comments on an earlier version of this manscript.

Data Availability Statement

Particulate organic carbon and inorganic carbon are from the MODIS satellite climatology served at NASA MODIS Climatology (NASA MODIS POC Climatology, 2020; Balch et al., 2005; Gordon et al., 2001; https://oceancolor.gsfc.nasa.gov/l3/). pCO_2 is taken from MPI-ULB-SOMFFN climatological product (Landschützer et al. 2020b). Following HG23, observations of temperature, salinity, nitrate, phosphate, and silicate are taken from the World Ocean Atlas (Garcia et al., 2019; Locarnini et al., 2019; Zweng et al., 2019). Shortwave radiation is taken from the WHOI OAFlux data set (Yu et al., 2006). Upwelling data are taken from ECCO Consortium (2021a). A compiled (climatologically averaged and aligned) data set plus a script to generate the random forest and sensitivities will be available on Zenodo.

References

Archer, D., Winguth, A., Lea, D., & Mahowald, N. (2000). What caused the glacial/interglacial atmospheric pCO2 cycles? Reviews of Geophysics, 38(2), 159–189. https://doi.org/10.1029/1999RG000066

Balch, W. M., Howard R. Gordon, B. C. Bowler, D. T. Drapeau, and E. S. Booth. (2005). Calcium carbonate measurements in the surface global ocean based on Moderate-Resolution Imaging Spectroradiometer data. Journal of Geophysical Research: Oceans 110, no. C7. https://doi.org/10.1029/2004JC002560

Barber, R. T., & Hiscock, M. R. (2006). A rising tide lifts all phytoplankton: Growth response of other phytoplankton taxa in diatom-dominated blooms. Global Biogeochemical Cycles, 20(4). https://doi.org/10.1029/2006GB002726

Bonnet, S., Guieu, C., Bruyant, F., Prášil, O., Van Wambeke, F., Raimbault, P., et al. (2008). Nutrient limitation of primary productivity in the Southeast Pacific (BIOSOPE cruise). Biogeosciences, 5(1), 215–225. https://doi.org/10.5194/bg-5-215-2008

Boyd, P. W., Claustre, H., Levy, M., Siegel, D. A., & Weber, T. (2019). Multi-faceted particle pumps drive carbon sequestration in the ocean. Nature, 568(7752), 327–335. https://doi.org/10.1038/s41586-019-1098-2

Breiman, L. (2001). Random Forests. Machine Learning, 45, 5–32. https://doi.org/10.1023/A:1010933404324

Brovkin, V., Lorenz, S., Raddatz, T., Ilyina, T., Stemmler, I., Toohey, M., & Claussen, M. (2019). What was the source of the atmospheric CO increase during the Holocene? Biogeosciences, 16(13), 2543–2555. https://doi.org/10.5194/bg-16-2543-2019

ECCO Consortium, Fukumori, I., Wang, O., Fenty, I., Forget, G., Heimbach, P., & Ponte, R. M. (2021a). ECCO central estimate (version 4 release 4) [Dataset]. Retrieved from https://podaac.jpl.nasa.gov/dataset/ECCO_L4_OCEAN_VEL_05DEG_MONTHLY_V4R4

ECCO Consortium, Fukumori, I., Wang, O., Fenty, I., Forget, G., Heimbach, P., & Ponte, R. M. (2021b). Synopsis of the ECCO central produc- tion global ocean and sea-ice state estimate, version 4 Release 4 [Dataset]. Zenodo. https://doi.org/10.5281/zenodo.4533349

Forget, G., Campin, J.-M., Heimbach, P., Hill, C. N., Ponte, R. M., & Wunsch, C. (2015). ECCO version 4: an integrated framework for non-linear inverse modeling and global ocean state estimation. Geoscientific Model Development, 8(10), 3071–3104. https://doi.org/10.5194/gmd-8-3071-2015

Garcia, H. E., Weathers, K. W., Paver, C. R., Smolyar, I., Boyer, T. P., Locarnini, et al. (2019). World Ocean Atlas 2018, Volume 4: Dissolved inorganic nutrients (phosphate, nitrate and nitrate+nitrite, silicate. Retrieved from https://www.ncei.noaa.gov/access/world-ocean-atlas-2018/bin/woa18.pl

Gordon, Howard R., G. Chris Boynton, William M. Balch, Stephen B. Groom, Derek S. Harbour, and Tim J. Smyth. (2001). Retrieval of coccolithophore calcite concentration from SeaWiFS imagery. Geophysical Research Letters 28, no. 8: 1587-1590. https://doi.org/10.1029/2000GL012025

Holder, C., & Gnanadesikan, A. (2021). Can machine learning extract the mechanisms controlling phytoplankton growth from large-scale observations? – A proof-of-concept study. Biogeosciences, 18(6), 1941–1970. https://doi.org/10.5194/bg-18-1941-2021

Holder, C., & Gnanadesikan, A. (2023). How Well do Earth System Models Capture Apparent Relationships Between Phytoplankton Biomass and Environmental Variables? Global Biogeochemical Cycles, 37(7). https://doi.org/10.1029/2023GB007701

Hopkins, J., Henson, S. A., Painter, S. C., Tyrrell, T., & Poulton, A. J. (2015). Phenological characteristics of global coccolithophore blooms. Global Biogeochemical Cycles, 29(2), 239–253. https://doi.org/10.1002/2014GB004919

Kemp, A. E. S., & Villareal, T. A. (2013). High diatom production and export in stratified waters – A potential negative feedback to global warming. Progress in Oceanography, 119, 4–23. https://doi.org/10.1016/j.pocean.2013.06.004

Klaas, C., & Archer, D. E. (2002). Association of sinking organic matter with various types of mineral ballast in the deep sea: Implications for the rain ratio. Global Biogeochemical Cycles, 16(4). https://doi.org/10.1029/2001GB001765

Krumhardt, K. M., Lovenduski, N. S., Iglesias-Rodriguez, M. D., & Kleypas, J. A. (2017). Coccolithophore growth and calcification in a changing ocean. Progress in Oceanography, 159, 276–295. https://doi.org/10.1016/j.pocean.2017.10.007

Kwon, E.Y., Primeau, F. and Sarmiento, J.L., 2009. The impact of remineralization depth on the air–sea carbon balance. Nature Geoscience, 2(9), 630-635. https://doi.org/10.1038/ngeo612

Landschützer, P., Laruelle, G. G., Roobaert, A., & Regnier, P. (2020). A uniform pCO2 climatology combining open and coastal oceans. Earth System Science Data, 12(4), 2537–2553. https://doi.org/10.5194/essd-12-2537-2020

Locarnini, R. A., Mishonov, A. V., Baranova, O. K., Boyer, T. P., Zweng, M. M., Garcia, et al. (2019). World Ocean Atlas 2018, Volume 1:Temperature. Retrieved from https://www.ncei.noaa.gov/access/world-ocean-atlas-2018/bin/woa18.pl

Liang, W., Han, J., Ge, Y., Zhu, W., Yang, J., & Liu, C. (2023). High-efficiency utilization of biomass and seawater resources based on a distributed system with SOFC-assisted CO2 capture:

Feasibility analysis and optimization. Energy Conversion and Management, 296, 117675. https://doi.org/10.1016/j.enconman.2023.117675

Iglesias-Rodríguez, M.D., Brown, C.W., Doney, S.C., Kleypas, J., Kolber, D., Kolber, Z., Hayes, P.K. and Falkowski, P.G., (2002). Representing key phytoplankton functional groups in ocean carbon cycle models: Coccolithophorids. Global Biogeochemical Cycles, 16(4), 47-1. https://doi.org/10.1029/2001GB001454

Margalef, R. (1978). Life-forms of phytoplankton as survival alternatives in an unstable environment. Oceanologica Acta, 1(4), 493–509.

Rivero-Calle, S., Gnanadesikan, A., Del Castillo, C. E., Balch, W. M., & Guikema, S. D. (2015). Multidecadal increase in North Atlantic coccolithophores and the potential role of rising CO 2. Science, 350(6267), 1533–1537. https://doi.org/10.1126/science.aaa8026

Sarmiento, J. L., & Gruber, N. (2002). Sinks for Anthropogenic Carbon. Physics Today, 55(8), 30–36. https://doi.org/10.1063/1.1510279

Stramski, D., Reynolds, R. A., Babin, M., Kaczmarek, S., Lewis, M. R., Röttgers, R., et al. (2008). Relationships between the surface concentration of particulate organic carbon and optical properties in the eastern South Pacific and eastern Atlantic Oceans. Biogeosciences, 5(1), 171–201. https://doi.org/10.5194/bg-5-171-2008

Yu, L., Jin, X., & Weller, R. A. (2006). Objectively analyzed Air-Sea Fluxes (OAFlux) for global oceans [Dataset]. Research Data Archive at the National Center for Atmospheric Research, Computational and Information Systems Laboratory. https://doi.org/10.5065/0JDQ-FP94

Zweng, M. M., Reagan, J. R., Seidov, D., Boyer, T. P., Locarnini, R. A., Garcia, et al. (2019). World Ocean Atlas 2018, Volume 2: Salinity. Retrieved from https://www.ncei.noaa.gov/access/world-ocean-atlas-2018/bin/woa18.pl